Medication discrepancies across multiple care transitions: A retrospective longitudinal cohort study in Italy

Transportation Engineering 18 (2024) 100278

Contents lists available at ScienceDirect

Transportation Engineering

journal homepage: www.sciencedirect.com/journal/transportation-engineering

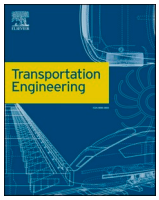

Human-powered vehicles as a way to abate transport-related greenhouse gas emissions: Part 2 - A virtual prototype for emissions and performance analyses

Alessandro Di Gesù, Chiara Gastaldi *, Cristiana Delprete

Department of Mechanical and Aerospace Engineering, Politecnico di Torino, Corso Duca degli Abruzzi 24, Torino, 10129, Italy

ARTICLE INFO

Keywords:
Velomobile
Model based system engineering
Customer need
Vehicle simulation
Virtual prototype
Digital twin
Experimental data
Greenhouse gas emission

ABSTRACT

Velomobiles, despite their potential for efficient transportation, remain relatively unknown compared to electric cars, receiving limited attention in academic research and public awareness. This paper highlights their untapped potential and underlines public interest in their adoption, provided a velomobile meeting customer requirements is available. Leveraging the Model Based System Engineering (MBSE) methodology, this work presents a structured approach to design, focusing on customer needs translation and digital prototype validation. This iterative process ensures velomobiles meet performance criteria while minimizing environmental impact. The lack of standardized testing for the energy consumption of Human-Powered Vehicles (HPVs) is addressed by proposing an analysis of consumption under diverse operating conditions, giving information on the environmental assessments. This study underscores velomobiles' potential as a sustainable transportation solution and provides a framework for their design, validation, and optimization.

1. Introduction

Velomobiles are a very efficient class of enclosed Human-Powered Vehicles (HPVs) which offer weather and impact protection in case of an accident [1]. Velomobiles are definitely not a hot topic these days. While writing this paper, a search for the keyword "velomobile" on Google Scholar over the past 12 months brings up only 12 results. In contrast, "electric car", generates 5360 results. The lack of research in this field can be related to velomobiles being mostly unknown among the general public, especially when compared to the vastly advertised electric cars. Only a few producers of velomobiles are well known in the velomobile community, and the most productive one manufactured less than 2000 vehicles over a 24-years span, between years 2000 and 2023 [2].

However, velomobiles display a hidden potential. As previously shown by the authors [3], once people are made aware of the existence of velomobiles, they may be very attracted by this technology. Many would even start using the velomobile as their primary mode of transportation for trips of routine, if the possibility arose. The same study also performs a comparative Life Cycle Assessment (LCA) to address the positive ecological impacts of the modal shift to velomobiles. The analysis, however, is based on the assumption that a velomobile capable of driving that modal shift could actually be produced. Table 1 displays a list of velomobiles currently available on the market. They are usually quite lightweight when compared to cars, or even mopeds, but are still far heavier than regular non-faired bicycles. Therefore, many come with pedal assistance, either fully integrated or optional, while just a few older models are solely designed for muscular propulsion. Velomobiles are also quite narrow, in order to travel on cycle paths, and generally display a low profile, the majority being no taller than 1200 mm, and many falling even shorter than 1000 mm (Fig. 1). In contrast, a car typically stands at 1400 mm tall, or taller. This height can deter individuals from using a low profile velomobile in densely populated areas where visibility may not be optimal. Consequently, in urban settings, a vehicle with a low profile could be perceived as risky to ride due to reduced visibility. This may not be a problem per se, since velomobiles excel on rural roads, where their higher top-end speed makes them a valuable alternative to either a bicycle or a car. However, the diminished height becomes problematic for individuals with mixed travel itineraries, encompassing rural roads for most of the journey, with the final kilometres traversing urban areas. These individuals are likely to opt against using a velomobile altogether, rather than utilizing it solely for part of the journey. Hence, a low-profile velomobile emerges as a viable mode of transportation primarily for those exclusively travelling on rural roads. However, in 2021, almost 38.9% of the European

* Corresponding author.
E-mail address: chiara.gastaldi@polito.it (C. Gastaldi).

https://doi.org/10.1016/j.treng.2024.100278
Received 6 April 2024; Received in revised form 8 August 2024; Accepted 24 September 2024
Available online 26 September 2024

Nomenclature

A:	mass distribution on the front axle (values normalized as a fraction of the total mass M), (measured in kg/kg)
C_{rr} :	coefficient of rolling resistance, (measured in N/N)
C_d :	coefficient of drag, (measured in N/N)
F:	force, (measured in N)
I:	moment of inertia, (measured in $kg{\cdot}m^2$)
M:	total mass of velomobile and riders, (measured in kg)
R_c :	radius of the clincher after deformation due to the static load, (measured in m)
T:	torque, (measured in N·m)
a :	quadratic term of the aerodynamic resistance, (measured in $N/(m^2/s^2)$)
b :	linear term of the aerodynamic resistance, (measured in $N/(m/s)$)
g:	constant of gravity, (9.81 m/s^2)
h:	height of the velomobile, (measured in m)
l:	length of the velomobile, (measured in m)
m:	mass of the velomobile, (measured in kg)
u:	parameter of rolling friction, (measured in m)
w:	width of the velomobile, (measured in m)
x:	distance, position, (measured in m)
$\dot{x}$:	linear speed, (measured in m/s)
$\ddot{x}$:	linear acceleration, (measured in m/s^2)
α :	slope, (measured in m/m)
η :	efficiency, (measured in W/W)
ω:	angular speed, (measured in rad/s)
$\dot{\omega}$:	angular acceleration, (measured in rad/s^2)

population lived in cities, 35.9% lived in smaller towns or suburbs, and only the remaining 25.2% resided in rural areas [4]. Although a quarter of the population is quite a relevant share of people, one should note that cities usually attract many daily commuters from rural areas for work, study or other services. Therefore, a taller velomobile is likely to be the best option for making velomobiles appealing to the general public.

At this juncture, one might wonder why most velomobiles are designed with a low profile. The rationale behind this choice is to accommodate a key customer requirement: the ability to attain a certain speed. Velomobiles belong to the category of Human-Powered Vehicles (HPVs), primarily propelled by human effort, though they can also feature electric assistance, as detailed in Table 1. However, legislative regulations stipulate that electric assistance is limited to 25 km/h in many European countries. Beyond this threshold, velomobiles must rely solely on human power. Yet, the human body's power output is limited, making it difficult for many individuals to sustain speeds of 25 km/h on flat terrain without electric assistance, even on a standard bicycle. Research demonstrates that aerodynamic resistance becomes the primary source of energy dissipation on a traditional bicycle, particularly above 15 km/h, escalating significantly beyond 25 km/h [5–7]. Particularly, the aerodynamic resistance F_{aero_x} can be mathematically represented by Eq. (1), where the C_d (drag coefficient) is a lump parameter that synthesises the aerodynamic performance of a certain shape. The other parameters involved in the equation are the air density ρ, the speed $\dot{x}$ and the frontal area A_f.

$$F_{aero_x} = \frac{1}{2}\,\rho{\cdot}C_d{\cdot}A_f{\cdot}\dot{x}^2 \tag{1}$$

Consequently, assuming certain weather conditions (i.e., fixed ρ), the aerodynamic resistance applied to a vehicle running at a certain speed $\dot{x}$ is solely defined by the shape of the vehicle (i.e., its C_d), and by a scaling factor proportional to the frontal area (i.e., A_f). For this reason, even if the vehicle is not exceptionally aerodynamic, a small frontal area can help to reduce the total drag force. Additionally, making the vehicle shorter in the vertical dimension (i.e., "less tall"), also allows to have a shorter - but equally streamlined - vehicle in the longitudinal direction (i.e., "less long"), possibly resulting in a more lightweight and handier velomobile. An alternative way to achieve low aerodynamic resistance,

Table 1
Main characteristics of 26 commercial velomobiles. In the first row: h is the height, l is the length, m is the mass, and w is the width of the velomobile. In the last column, MP: muscular propulsion; PA: pedal assistance, fully integrated in the design; MP-PA: basic design with MP, but optional PA available.

Manufacturer	model	h/mm	l/mm	m/kg	w/mm	propulsion
Better Bike	Pebl	1500	2590	104	1220	PA
city q	–	1550	2220	68	870	PA
Drymer	Business	1680	2010	–	840	MP-PA
eqhawk	–	1120	2820	75	880	PA
Flevobike	Orca	940	2430	39.5	780	MP-PA
Grant Sinclair	IRIS	1280	2600	–	940	PA
Katanga	WAW	870	2870	–	690	MP-PA
Kinner	–	–	2200	–	1000	PA
Leiba	classic	1170	2170	35	870	MP
Leiba	classic L	1205	2760	49–55	880	MP-PA
Leiba	hybrid	1070	2560	53	890	PA
Leiba	rekord	865	2723	26.5	710	MP
Leiba	x-stream	1040	2560	33.5	810	MP
Leitra	Leitra	1200–1400	2050	30	980	MP-PA
Pod Bike	Frikar e_bike	1190	2360	90	839	PA
Pod Ride	–	1440	1960	70	750	PA
QuadVelo	–	1330	2500	85	850	PA
Sinner Bikes	Hilgo	880	2440	30	720	MP-PA
Sinner Bikes	Mango Plus	950	2450	32.5	750	MP-PA
Sinner Bikes	Mango Sport	930	2450	27.5	730	MP-PA
Sinner Bikes	Mango Tour	950	2450	32.5	800	MP-PA
Veemo	–	1500	2000	–	890	PA
Velomobiel	Quattrovelo	880	2835	35	770	MP-PA
Velomobiel	Quest	900	2850	34	765	MP-PA
Velomobiel	Quest Xs	855	2600	31	765	MP
Velomobiel	Strada	895	2650	34.5	800	MP

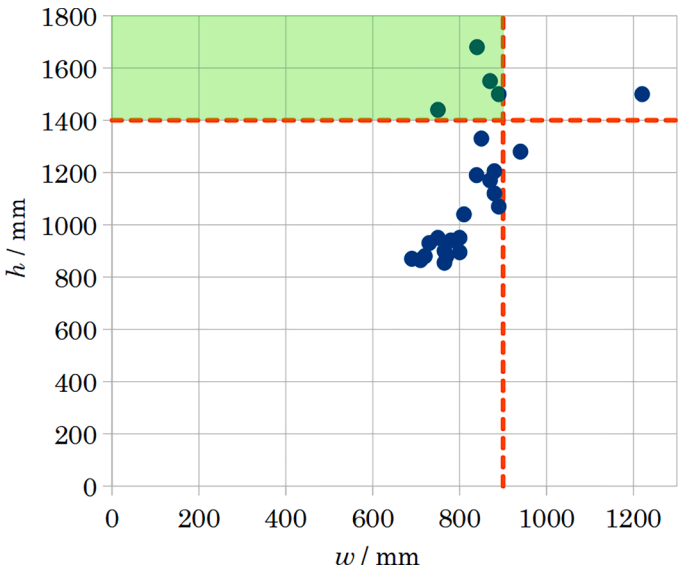

Fig. 1. Only 4 out of the 26 commercial velomobiles analysed are both narrow and tall.

while still keeping a taller profile, is to minimise the drag, i.e. acting on C_d rather than A_f. To the best of the authors' knowledge, this approach has not been properly investigated yet. In fact, the tallest velomobiles reported in Table 1 are either:

- heavy cargo vehicles and/or
- partially enclosed vehicles, or
- very short vehicles (below 2 metres)

each of which is attributable to the bluff bodies category, certainly not optimised for drag minimisation.

The present work serves to demonstrate that a modal shift which encompasses the adoption of a new mobility alternative is possible, when following a structured process like the Model Based System Engineering (MBSE) methodology to guide the design phase. Specifically, as shown in Sections 2.1–2.2, a pre-emptive survey was utilized to identify customer needs, which were then translated into measurable and verifiable design requirements. The allocation and verification of these requirements in subsequent design phases ensure the resulting product aligns with customer needs, thereby facilitating the modal shift. Furthermore, MBSE leverages digital artifacts, such as virtual prototypes, which can be supplemented with experimental data, thus becoming digital twins [8]. Depending on whether the integration with experimental data is performed offline [9,10] or online [11–13], the digital twin may be used for scenario evaluation and/or for monitoring purposes. A notable contribution of this study is the development of a model used both as a virtual prototype for the velomobile (see Section 2.3), and later validated as an offline digital twin against experimental data gathered from existing vehicles (see Section 3.1). A future evolution of the present model could involve the modeling of specific critical components using real-time data measured on the velomobile ("online digital twin") for monitoring purposes and to assist users in scheduling maintenance. However, this has not been introduced in the present paper, as such an analysis is beyond the scope of this study.

These virtual prototypes, when used for scenario evaluation (as in Section 3.2) are a vital part of the design process as they allow the exploration of:

- different boundary (i.e. working) conditions;
- different combinations of design parameters.

By establishing various boundary conditions and analyzing how the vehicle responds to changes, one can effectively perform verification & validation and optimize its performance. For instance, if a requirement involves achieving a specific speed with a fixed power input from the rider(s), it is essential to ensure that power dissipation does not exceed a certain threshold, which depends on factors such as terrain slope. To stay within this limit, one can explore different configurations and assess their performance, considering parameters like rolling resistance and aerodynamics. Initially, these influences can be studied independently before evaluating their combined impact. Such exploration is particularly relevant in the case of HPVs not only for design and optimization purposes, but also to assess the environmental impact of the use phase of the velomobile. In fact, HPVs lack a standardised testing cycle for the evaluation of the energy consumption as is the case with cars. To overcome this issue, it is here proposed to analyse the consumption data of the validated virtual prototype of the velomobile run in an ample spectrum of possible working conditions. The output has been used in [3] to perform a Comparative Life Cycle Assessment.

2. Methodology

2.1. Model based system engineering

The velomobile analysed in the present work is being developed according to the MBSE methodology widely adopted in the aerospace and automotive industries [14]. MBSE is a structured holistic approach which "focuses on defining customer needs and required functionality early in the development cycle, documenting requirements, then proceeding with design synthesis and system validation while considering the complete problem" [15]. A typical graphical representation of the system development process is the "V" diagram. In it, the left leg represents the design phase starting from customer requirements and ending with component manufacturing, while the right leg corresponds to testing, validation and commissioning. The hierarchical structure implies starting with the overall system (top) and then delving into the design specifics of its components and parts (bottom), favouring a top-down methodology. The "V" structure of the diagram underlines the importance of aligning each design action on the left side with its production counterpart depicted on the right side. In this classical framework, verification and validation occur on physical prototypes. The classical "V" model can be expanded to include virtual prototyping [8], thus yielding a "W" shape as shown in Fig. 2. To elaborate further, the initial conceptual design phase (first descending leg) can be distinguished from the virtual modelling (first ascending leg) and detailed design specification (second descending leg) phases. In this scenario, a dedicated virtual prototyping stage (i.e. physics-based models development and verification) precedes the physical testing and validation phase. The virtual prototypes then serve as the foundation for generating the digital twin enhanced with data collected from product testing and commissioning (second ascending leg) to create a product-specific digital twin. The digital twin which is then validated as the conclusion of the digital twin cycle. This initial validation is necessary; in fact, the digital twin must undergo periodic re-validation throughout its lifecycle to maintain its reliability. In this context, the principal objective of the digital twin is to mitigate uncertainties by integrating component/subsystem data and, whenever feasible, streamline the testing and validation phase for the entire system by reducing assumed uncertainties. Another critical consideration is how the digital twin will transition into the asset management phase, which will be discussed subsequently. In this paper, a physics-based model of a Human Powered Vehicle is presented to serve multiple purposes, as outlined below and further shown in Fig. 2.

- The model has been used to serve as a virtual prototype for the soft mobility velomobile described in Section 1. As previously discussed, such prototype is the key to perform virtual design validation, i.e. checking that the design solution identified through the conceptual

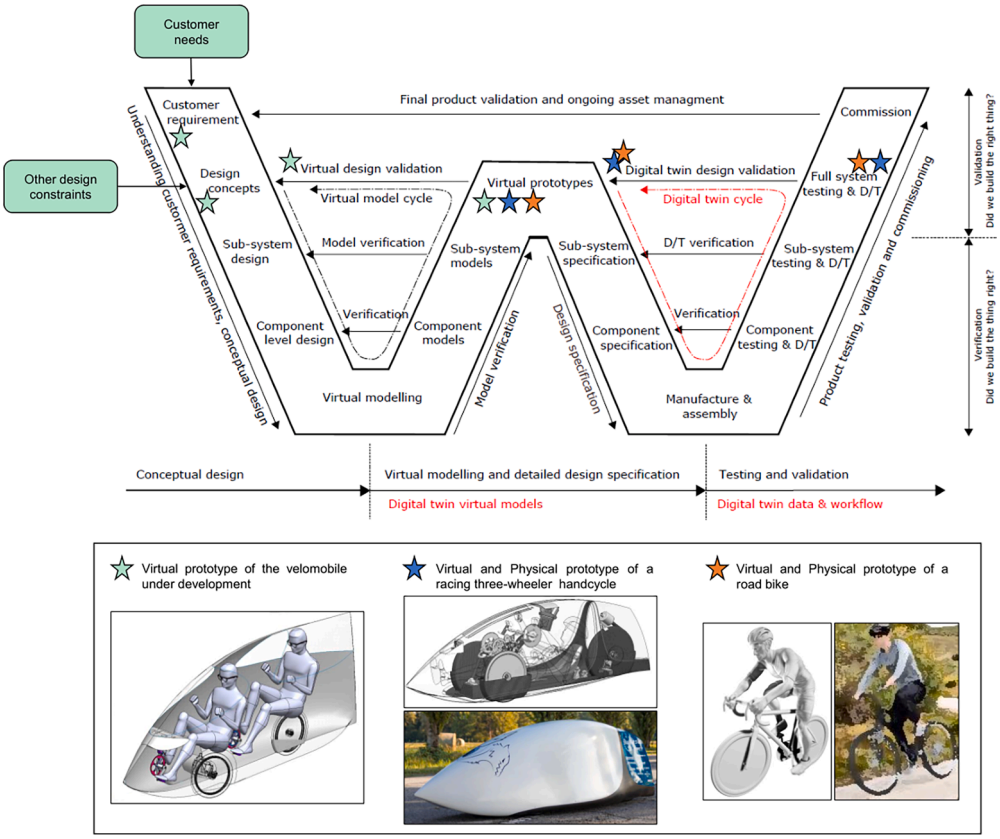

Fig. 2. Application of the MBSE methodology to the velomobile case study - adapted from Wagg et al. [8].

design phase meets all prescribed requirements. At this preliminary stage, traceability is already implemented, ensuring that the design parameters in the virtual prototype align with customer requirements through appropriate constraints. Additionally, the automated evaluation of the analyses' results with control parameters derived by the requirements allows for a straightforward feedback. The virtual prototype can, furthermore, be used to characterize the design in terms of energy consumption, useful for life cycle assessment analyses.

- The model can be adapted to depict various types of HPVs, such as a road bike and a racing handcycle, as depicted in Fig. 2. In both scenarios, there exists a physical prototype. Experimental data are employed to elevate the virtual prototype to the status of a digital twin. This initial validation serves to confirm the reliability of the virtual prototype. Additionally, the resulting digital twin holds particular significance for the high-speed velomobile, where it can facilitate uncertainty quantification and asset management before competitions with unfamiliar boundary conditions, such as varying weather or different tracks.

The HPV model is thoroughly outlined in Section 2.3 for the velomobile case. The adjustments necessary to tailor the model to represent different types of HPVs, such as racing handcycles and road bikes, will be emphasized in Section 3.1. Model validation procedures conducted on the racing handcycle and road bike are detailed in Section 3.1. In Section 3.2, the outcomes related to the velomobile virtual prototype are presented. These findings establish a framework for evaluating the velomobile's energy consumption as a mobility solution and perform the verification of the primary design constraints outlined in Section 2.2.

2.2. MoSToVIt survey and design constraints

According to MBSE, the design process should start with the retrieval of customer needs. To be more precise, MBSE actually invites designers to consider the needs of all relevant stakeholders, including regulatory bodies, manufacturers, industry experts, market analysts, and others. While we do consider secondary stakeholders, such as legislative bodies (as will be explained later in this section), the present study mainly focuses on customer needs and their connection to the velomobile features and performance. Other relevant requirements and stakeholders, such as those connected to manufacturing and cost, are outside the scope of this preliminary study. However, some relevant information on the price people would be willing to pay for a velomobile, along with an analysis of the impact of velomobile price variability on people's willingness to adopt them, can be found in the companion article of this study [3]. Customer needs related to the velomobile technical features and expected performance were derived from the analysis of responses collected through the MoSToVIt survey ("Modal Shift To Velomobiles in Italy"), which received 1291 responses. The 2 aims of the survey were:

1. to analyse commuting patterns and assess the impact of a transition from the participants' present modes of transport to the use of the velomobile;
2. to establish the foundation for the velomobile's actual design.

The first analysis, conducted with a comparative life cycle assessment (LCA), is detailed in a companion article [3], while this paper focuses on the second analysis.

Survey participants evaluated 27 velomobile characteristics, providing both quantitative and qualitative (1 to 5 stars) feedback. In this instance, only the answers of the MoSToVIt respondents who declared to be favourable to the modal shift to the velomobile were considered. However, the average values did not show significant changes even when answers from "non-users" were included. This is because "non-users," i.e., survey respondents who declared they were unwilling to adopt the velomobile due to their specific lifestyle (long

traveling distances, need to accompany more than one passenger, etc.), gave similar responses regarding the characteristics they would like a velomobile to have. An aggregated analysis of this data guided the definition of design requirements, i.e. measurable and verifiable constraints. Table 2 outlines key customer needs translating into design requirements. Main aspects include the vehicle's aerodynamics, size, electric assistance and possibility to accommodate a passenger (who can also power the velomobile in tandem) together with the rider. While some customer needs can be directly translated to design parameters (e.g., luggage compartment volume), others, especially qualitative aspects like the possibility to drive on preferred terrain types, offered valuable insights for the velomobile's advanced design phase. Another customer need that cannot be directly translated into a design parameter, despite having a quantitative answer (i.e. 37.8 km/h) is the required speed on flat ground. This happens because the required speed is a function of many factors which include design parameters (vehicle weight, aerodynamic profile, etc.) and boundary conditions (terrain type, human power). As shown in Fig. 3, only verification through a virtual prototype can ensure that the chosen set of design parameters meets the requirement. Nevertheless it is vital to stress that verification of requirements is meaningful only if the boundary conditions are representative of typical working conditions. The required speed on flat ground, taken here as an example, is influenced by the power source, which is solely human for speeds higher than 25 km/h according to Italian regulations. It is therefore necessary to estimate the power that the average person can provide. As addressed in [5], cycling performance involves many factors, including peak power output, preferred cadence (which is related to the recruitment of different types of muscle fibres), pacing strategy and more. Therefore, the problem was addressed in a simplified yet reasonable way. By using two simulators for cycling performance [16,17] it was assessed that with 100 W of constant power, the cruising speed on a bicycle falls in the 21-to-25 km/h interval. As this was considered by the authors a range of speed which can be sustained by an average person, 100 W was used as the reference power representative of an average person. This conclusion was also reached considering the speed dependency of a cyclist from the VO_2max (i.e., the maximum amount of oxygen that an individual can utilize during intense exercise). In fact, [18] shows that depending on the age and sex, 20-to-40 ml/min/kg represent a reasonable average fitness level. Assuming a 70 kg person, with 30 ml/min/kg of VO_2max, the VO_2 flux is set to 2.1 l/min, which is enough to power a bicycle between 6 m/s and 7 m/s [19]. The design phase includes, however, also constraints which do not come from customer needs, but are derived from other sources. For example, as shown in Table 3 the width and height of the velomobile are set by customer requirements. However, the Italian legislation states that a velocipede can be no longer than 3.5 metres. Therefore, the overall volume of the velomobile (the working volume for the design of the velomobile's fairing) is completely defined when considering both the customer needs and legislative requirements. This process is extended also to other design features, to define a comprehensive starting point for the complete design of the vehicle (Fig. 3).

Table 2
Results of the most relevant parameters for the preliminary design, assessed through the MoSToVIt survey. In the "unit" column, the symbol ★ denotes the level of relevance of the customer need according to the people interviewed (maximum value 5★).

Customer need	avg. value	st. dev.	unit	influence on	design constraint
Luggage compartment volume	156.36	63.72	L	aerodynamics	150 l of luggage
Passenger adult	3.22	1.47	★		it must be possible to ride the velomobile
Passenger child	3.10	1.62	★		either alone or in tandem
Ride on cycle paths	3.44	1.44	★		usage on cycle path is important. Maximum width should be no more than 900 mm
Ride on road among motorised vehicles	4.35	0.96	★		usage on open roads is very important; hence, a 1400 mm height is required for visibility
Speed on flat ground	37.78	10.09	km/h		when powered with 100 W/riders, the vehicle should provide a cruising speed of 35–40 km/h
Stability while at a stop without putting feet down	4.30	1.05	★		at least 3 wheels are needed
Electric assistance importance	4.06	1.16	★	electric assistance	electric assistance must be implemented
Speed uphill (25 km/h)	3.43	1.33	★		

2.3. Virtual prototype of the velomobile

This section presents the physics-based model used as virtual prototype and digital twin of HPVs, such as velomobile, road bike and racing handcycle. The model has been developed in Simulink® (MATLAB®-based graphical programming environment). The model can be broken down in the following eight main subsystems, which encompass both vehicle characteristics and boundary conditions:

1. the aerodynamics of the vehicle;
2. the rolling resistance;
3. the terrain slope;
4. the vehicle's inertia (both linear for the chassis and rotational for the wheels);
5. the braking action;
6. the electric assistance;
7. the number of riders and their power output;
8. the gear shifting system.

The different subsystems may be modified to tune the model to the different kinds of HPVs, e.g. the Electric Assistance block is bypassed in the case of the racing handcycle. In the following, the velomobile shall be used as an example to present the model, as it requires all the outlined subsystems. Fig. 4a shows the highest level of the block diagram (note that the inertia is a degenerate subsystem, represented by a simple gain). This model also allows the user to conduct a carbon footprint analysis (i.e., a LCA considering the global warming potential category only). The calculation is conducted accounting for the electric energy used by the motor, the caloric expenditure of the rider(s), and their associated emission factors (Fig. 4b). Specifically, for the caloric consumption-related emissions, the calculation can be conducted using a linear relation between the metabolic rate and the external power expressed by the riders [3].

2.3.1. Longitudinal equilibrium

Fig. 5 a shows the velomobile's free body diagram that was used to develop the Simulink model. The frame and the fairing were considered as a whole rigid body (i.e., no suspensions were included in the model) and only the forces that contribute to the horizontal translation of the

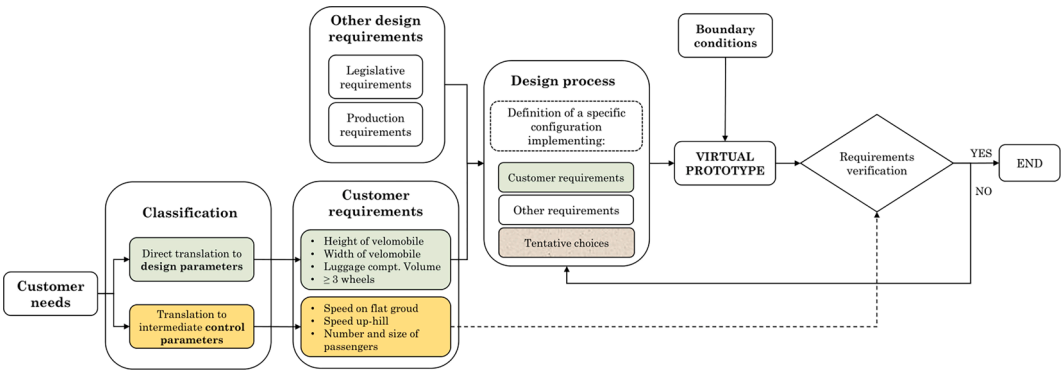

Fig. 3. Design workflow started with the translation of Customer Needs in design requirements.

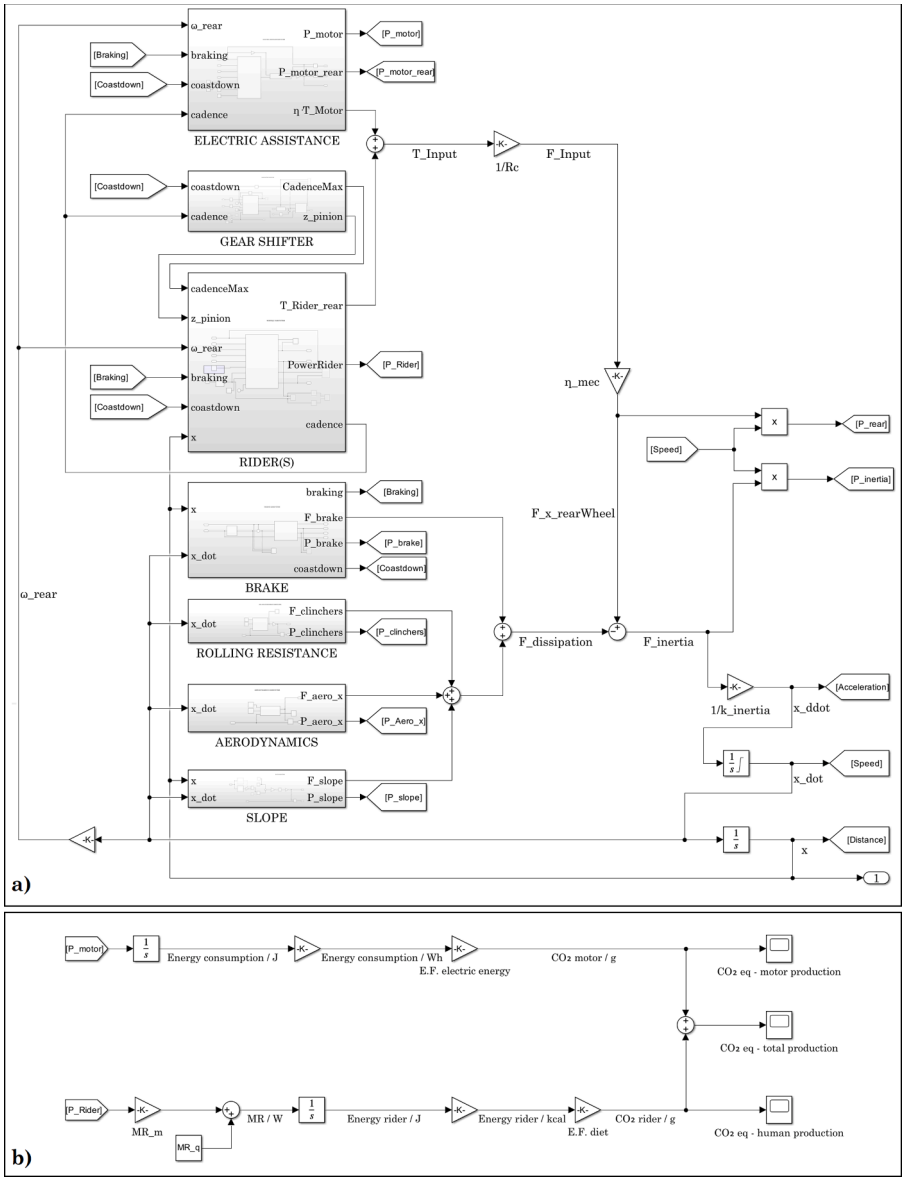

Fig. 4. Screenshot of the highest level of the Simulink model. a) Velomobile model. b) GHG emissions calculation. Note that the emission factor of the diet should also take into account the level replenishment of the calories expended, as explained in [3].

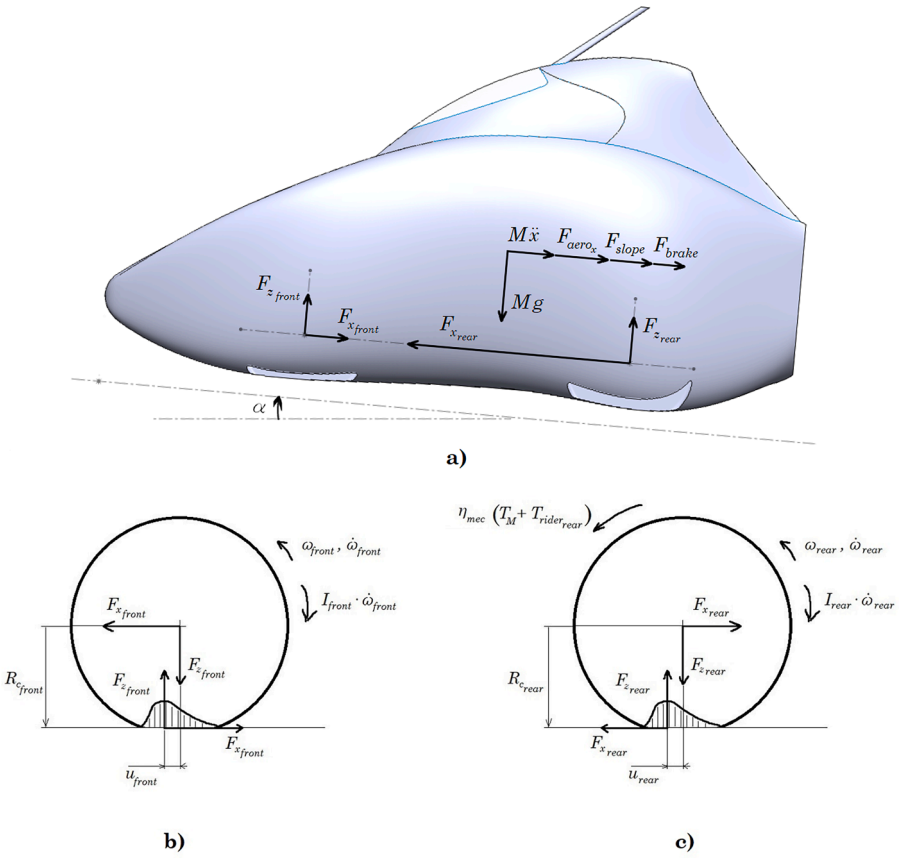

Fig. 5. **a)** Free body diagram of the velomobile representing a scheme of the forces applied to the velomobile. **b)** Free body diagram of the front axle. **c)** Free body diagram of the rear axle. Single-track equivalent representation, where each axle is condensed in an equivalent single wheel. This scheme could be used independently for a bicycle, a tricycle or a quadracycle. The bottom of each wheel shows a qualitative distribution of the contact pressure which generates the rolling resistance torque through the u parameter.

vehicle were taken into account. The model accounts for neither lateral dynamics (yaw and roll) nor for the pitching of the vehicle. The longitudinal equilibrium of the velomobile is expressed by Eq. (2).

$$M\ddot{x} + F_{aero_x} + F_{slope} + F_{brake} + F_{x_{front}} = F_{x_{rear}} \tag{2}$$

2.3.2. Rear wheel propulsive force $F_{x_{rear}}$

The constraint reaction applied by the rear wheel's hub to the frame is the propulsive force of the velomobile. Its mathematical formulation can be derived by analysing the free body diagram of the rear wheel (Fig. 5c) and writing the system of equations (Eq. 3) which represents the rotational equilibrium of the wheel. Once solved, $F_{x_{rear}}$ is given by Eq. (4). As reported in Table 3, most of the parameters involved in this equation are variable. Their modelisation is described in Section 2.3.8 to 2.3.11.

$$\begin{cases} (T_M + T_{rider_{rear}}) \cdot \eta_{mec} - F_{x_{rear}} \cdot R_{c_{rear}} - F_{z_{rear}} \cdot u_{rear} - I_{rear} \cdot \dot{\omega}_{rear} = 0 \\ F_{z_{rear}} = M \cdot g \cdot (1 - A) \\ \dfrac{u_{rear}}{R_{c_{rear}}} = C_{rr_{rear}} \end{cases} \tag{3}$$

$$F_{x_{rear}} = \frac{(T_M + T_{rider_{rear}}) \cdot \eta_{mec}}{R_{c_{rear}}} + M \cdot g \cdot (1 - A) \cdot C_{rr_{rear}} - \frac{I_{rear} \cdot \dot{\omega}_{rear}}{R_{c_{rear}}} \tag{4}$$

2.3.3. Front axle resistive force $F_{x_{front}}$

A similar analysis can be replicated for the front axle using Fig. 5.b to find the system in Eqs. (5) and (6).

$$\begin{cases} F_{x_{front}} \cdot R_{c_{front}} - F_{z_{front}} \cdot u_{front} - I_{rear} \cdot \dot{\omega}_{front} = 0 \\ F_{z_{front}} = M \cdot g \cdot A \\ \dfrac{u_{front}}{R_{c_{front}}} = C_{rr_{front}} \end{cases} \tag{5}$$

Table 3
Dependencies of the non-constant parameters in the model ("x" for dependent, "-" for independent).

	Instantaneous variability			Global variability			
	speed of the vehicle	cadence	gear engaged	fairing geometry	number of riders	average input power of a single rider	free parameter
C_{rr}	x	–	–	–	–	–	–
F_{aero_x}	x	–	–	x	–	–	–
M	–	–	–	–	x	–	–
T_M	x	–	–	–	–	–	–
$T_{rider_{rear}}$	x	x	x	–	x	x	–
α	–	–	–	–	–	–	x

$$F_{x_{front}} = M{\cdot}g{\cdot}A{\cdot}C_{rr_{front}} + \frac{I_{front}{\cdot}\dot{\omega}_{front}}{R_{c_{front}}} \tag{6}$$

2.3.4. Braking force F_{brake}

The braking force is physically applied to the wheels. Therefore, its effect should appear as two torques in the two free body diagrams of the axles (Fig. 5b-c). However, since in the model the combined effect is what matters, F_{brake} was modelled as a single resisting equivalent force acting on the main body of the vehicle (Fig. 5a). The numerical value of the force is modelled in the BRAKE subsystem of the Simulink model (Fig. 4) which is discussed in Section 2.3.12.

2.3.5. Slope force F_{slope}

The force due to the slope can be simply defined with Eq. (7). The value of α in the model can be expressed, through a vector, as a function of the distance travelled x. It can be resistive or propulsive, depending on the sign of α.

$$F_{slope} = M{\cdot}g{\cdot}\sin(\alpha) \tag{7}$$

2.3.6. Aerodynamic resistance F_{aero_x}

The aerodynamic resistance was modelled as a quadratic function of the linear speed of the velomobile (Eq. (8)). The model is detailed in Section 2.3.11.

$$F_{aero_x} = a\dot{x}^2 + b\dot{x} \tag{8}$$

2.3.7. Inertia: $\ddot{x}$ and $k_{inertia}$

The term $M\ddot{x}$ in Eq. (2) does not represent the whole inertia of the vehicle. In fact, it only represents the linear inertia. The total inertia is assessed by combining Eq. (2–4-6–7) and solving the system to find the linear acceleration (Eq. (9)). The inertia of the velomobile is then represented by the denominator of Eq. (9). Considering the same type of clinchers, and assuming a very low dependency of the C_{rr} from the vertical force applied to the wheel, the simplified Eq. (10) can be derived. Note that this is an approximation, because the real behaviour of the clinchers depends on the weight distribution [20]. However, since the velomobile design is still in the early stages, a more precise approach could not be integrated. Besides, since the model does not account for the suspensions dynamics, the actual instantaneous weight distribution could not have been assessed, anyway.

$$\ddot{x} = \frac{\frac{(T_M + T_{rider_{rear}})\cdot\eta_{mec}}{R_{crear}} - M{\cdot}g{\cdot}\left[C_{rr_{rear}} + A\left(C_{rr_{front}} - C_{rr_{rear}}\right)\right] - M{\cdot}g{\cdot}\sin(\alpha) - F_{aero_x} - F_{brake}}{M + \frac{I_{rear}}{R^2_{crear}} + \frac{I_{front}}{R^2_{cfront}}} \tag{9}$$

$$\ddot{x} = \frac{\frac{(T_M + T_{rider_{rear}})\cdot\eta_{mec}}{R_c} - M{\cdot}g{\cdot}C_{rr} - M{\cdot}g{\cdot}\sin(\alpha) - F_{aero_x} - F_{brake}}{M + \frac{I_{rear}+I_{front}}{R^2_c}} \tag{10}$$

The efficiency η_{mec} of the transmission (chains and pulleys) was set to 93%, which stands in the lower-end of the actual spectrum expected for this application [21,22]. The purpose of using a relatively low efficiency was to obtain conservative results from the simulations. The inertia parameters (i.e., the static and rotating masses) of the velomobile were defined on the basis of the experience of the authors, given the know-how acquired by the research group in designing these kind of vehicles since 2009 [23]. Each rider was assigned a mass of 70 kg. Table 3shows the variability of the non-constant parameters involved in Eq. (10) which will be analysed in the next paragraphs. Finally, Eq. (11) is a compact form of Eq. (10), where each term is rewritten as the output of the Simulink model's subsystems shown in Fig. 4.

$$\ddot{x} = \frac{\frac{T_{input}}{R_c}\cdot\eta_{mec} - F_{clinchers} - F_{slope} - F_{aero_x} - F_{brake}}{k_{inertia}} \tag{11}$$

2.3.8. Electric assistance subsystem

The velomobile is equipped with an electric motor to allow for a good acceleration when the vehicle starts from a standstill. Its torque T_M depends both on:

1. the mechanical and electrical characteristics of the motor, and
2. the legislative regulations.

The first dependency was accounted for by modelling the electric motor according to the ideal characteristic (i.e., constant torque in the first segment, and then constant power when the nominal power is reached) and applying a bulk efficiency of 85%. The producer of recumbent trikes and quadracycles *Outrider USA* reports an efficiency of 93% of their motor, claiming it to be the most efficient in the e-bike panorama [24]. Therefore, 85% seems ad adequate value for this application. As for the national regulations, the Italian legislation assesses that velocipedes may be *"equipped with an auxiliary electric motor having a maximum continuous rated power of 0.25 kW, or 0.5 kW if used for the transportation of goods"* and that *"the power supply of the motor must be progressively reduced and finally cut off when the vehicle reaches 25 km/h, or sooner if the cyclist stops pedalling"*. Consequently, the authors implemented in the model a function that respects these characteristics. The behaviour of the electric assistance can be seen in Fig. 6.

2.3.9. Rider(s) and gear shift subsystems

Though electrically assisted, the velomobile still pertains to the class of HPVs. As such, the power input of the rider is essential for its propulsion. As previously shown in Eq. (4), the rotational balance of the rear wheel depends on $T_{rider_{rear}}$ (i.e., the torque that the hub of the rear wheel receives from the riders).

However, as shown in Table 3, this torque depends on five other parameters. Specifically, under the assumption that the power input of the riders is the same, $T_{rider_{rear}}$ is directly proportional to the number of riders and to their power output. This can be referred to as a *global variability*, which changes from one simulation to another. However, $T_{rider_{rear}}$ also exhibits an *instantaneous variability*: it is directly proportional to the gear ratio (which is set through the gear engaged), and inversely proportional to the cadence. Still, these two parameters (i.e., the cadence and the gear engaged) are not independent from each other. Assuming constant power, right after a gear shift, the cadence drops and a transient is required for it to reach its plateau again. This is related to the acceleration of the vehicle, which is modelled through the $k_{inertia}$ parameter, as by Eq. 11. In the model, the gear shift occurs automatically when the cadence reaches two threshold limits: the lower one is used for downshifting (e.g. during a brake), while the higher one is used for up-shifting. The behaviour of the gear shift is reported in Fig. 6.

Finally, this torque also depends on the vehicle's speed (Table 3) due to the presence of a freewheel in the rear hub. When the wheel rotates faster than the sprocket (e.g., because the gear is too low, or the vehicle

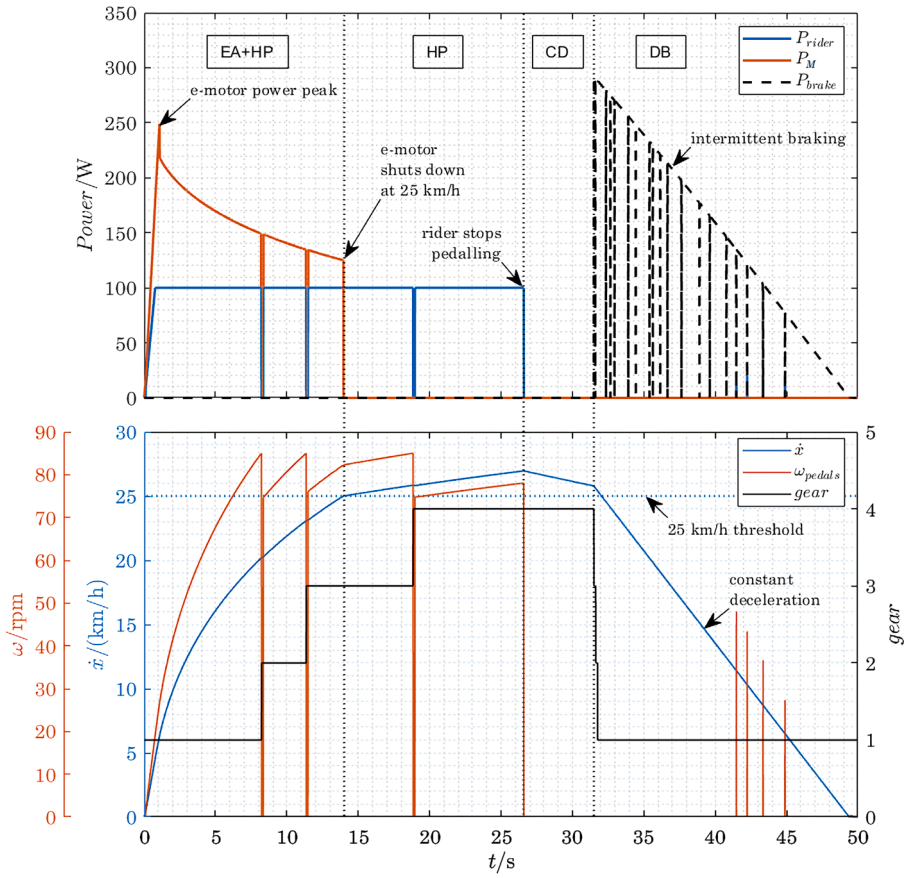

Fig. 6. Simulation of a start-and-stop, in which 4 phases can be identified: electric assistance and human power (EA+HP), human power only (HP), coast-down (CD), and dissipative braking (DB). Starting from a standstill, as soon as the rider starts to pedal, the motor kicks in. After peaking at 250 W, the power output of the motor decreases and is finally cut to 0 W at 25 km/h (around 14 s in the simulation). Here starts the HP phase, where the vehicle continues to accelerate thanks to the rider action, until the coast-down controller (see Section 2.3.12) is set to 1 and P_{rider} is set to 0 W. After a brief coast-down phase, the rider then starts to actively brake to keep an almost constant deceleration and reach a complete stop at the desired x_objective (see Section 2.3.12). The drops in P_{rider} and ω_{pedals} correspond to the gear shifts, when the chain is not engaged on the pinions and the rider is not transmitting any power to the wheels. The peaks in P_{rider} and ω_{pedals} during the DB phase are slight adjustments that the algorithm performs to stop the vehicle exactly at the desired x_obj while maintaining the maximum allowable deceleration.

is on a steep descent), the freewheel disengages and the torque transmitted to the rear wheel is null, even if the rider is still pedalling. This is implemented in the model within a function, in the "RIDER(S)" subsystem shown in Fig. 4. Furthermore, in order to avoid unreal peaks of $\ddot{x}$, the model introduces an upper limit of 50 $N{\cdot}m$ to the rider torque T_{rider}. This value corresponds to about 0.7 $N{\cdot}m/kg$ for a 70 kg person, which is roughly half of the value reported in [25] for elite male cyclists during a 4 min session (1.5 $N{\cdot}m/kg$).

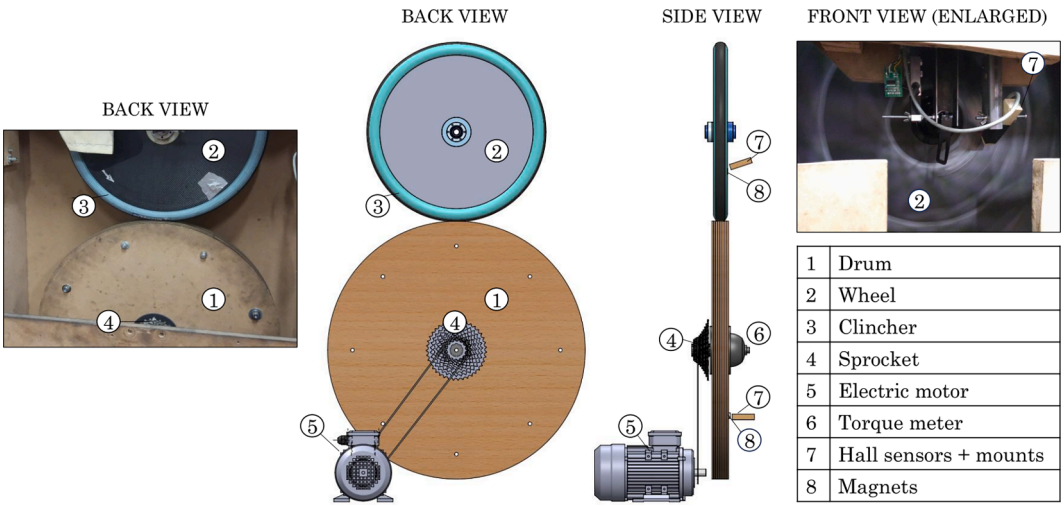

1	Drum
2	Wheel
3	Clincher
4	Sprocket
5	Electric motor
6	Torque meter
7	Hall sensors + mounts
8	Magnets

Fig. 7. Tyres test bench.

2.3.10. Simulink subsystem - Rolling resistance

The C_{rr} dependency from speed of the vehicle was directly input in the model as a quadratic function obtained from primary unpublished experimental data. These measurements were performed with an improved version of the test bench described in [26]. Unlike the old test bench, which had a minimum acquisition speed set to 45 km/h, the newer version could acquire good data even below 10 km/h. In this new configuration, the data acquired were: (1) the torque T_d at the drum's hub, measured with a PowerTap G3, and (2) the angular speed ω of the wheel, determined with a hall sensor. The tangential force F_x applied by the drum to keep the wheel into rotation was calculated dividing T_d by the radius of the drum R_d, as in Eq. (12). Finally, the C_{rr} was found with Eq. (13), knowing the vertical load F_z applied to the wheel. The free-body diagram of the wheel is the same as the one previously reported in Fig. 5 b.

$$F_x = \frac{T_d}{R_d} \tag{12}$$

$$C_{rr} = \frac{F_x}{F_z} \tag{13}$$

All the acquisitions were performed with the wheel in steady-state condition (i.e., with null average value of the tangential acceleration, during a 4 s measurement). For each type of clincher, the C_{rr} curve was obtained interpolating the data acquired at 11 fixed speeds, between 15 km/h and 145 km/h, under a vertical load of 412 N. Fig. 7 shows a scheme and two photos of the test bench.

2.3.11. Aerodynamics subsystem

As stated earlier in Section 2.2, the design of the velomobile was influenced by the answers collected in the MoSToVIt survey. The main aerodynamics requirements that derived from it were: (1) a cruising speed of 38 km/h, and (2) the possibility to transport a passenger. Therefore, the shape of the chassis was designed to accommodate 2 people while still maintaining a low drag coefficient. The CAD was drawn in SolidWorks®, and the aerodynamic analyses were performed with STAR-CCM+®. The CFD model developed in this paper capitalizes the experience of the authors within student team Policumbent projects[1] The procedure used to develop the model is solid and was validated experimentally with both (1) wind tunnel testing [27], and (2) accelerometer and odometer data acquisition and analysis [28]. A further check was performed by analysing a non-faired bicycle and finding comparable results with that of an independent calculator [16] which uses fixed C_d and frontal area values depending on the cyclist position. The simulations were conducted in steady-state conditions, with rotating wheels, still chassis and incoming headwind (Fig. 8). The analyses were performed at 15 km/h, 30 km/h, 40 km/h, 50 km/h and 70 km/h. The curves were generated interpolating these three data points with a quadratic function, forcing the intercept in the origin (i.e., imposing null drag dissipation when the vehicle is not moving).

2.3.12. Brake subsystem

The braking system of the model was designed to simulate a reasonable behaviour of the rider during the brake, in many different scenarios. For this reason, in this subsystem, one can set:

1. A defined number of stops along the trip;
2. The precise location of the stops;
3. The stopping time at each stop, to simulate different scenarios like: (i) giving the right of way, (ii) stopping at an intersection or (iii) at a red light;
4. The maximum allowable deceleration $\ddot{x}_{brake_{max}}$;
5. A controller for the coast-down of the vehicle.

The number and position of each stop is defined through the vector `x_objective`, whose values represent the distance of the stop from the beginning of the trip. For example, the vector [300 420 700] forces the vehicle to stop a first time after 300 m, then a second time after another 120 m (for a total of 420 m), and finally a third time after another 280 m (for a total of 700 m).

The stopping time is modeled via the `t_still` vector, of the same dimension as `x_objective`, whose values expressed in seconds represent the waiting time of the vehicle at each stop. When the value is set to zero (e.g., in the second stop of vector [5 0 15]) the stop is not ignored: the vehicle simply stops at the intended point set by `x_objective` and starts right away once again.

The maximum allowable deceleration is used to calculate the onset of the brake x_{brake} (i.e., the x value at which the braking is to begin). Past that point, the vehicle slows at a constant deceleration of $\ddot{x}_{brake_{max}}$. This phase can be preceded by a coast-down phase, which can be set through the Δ`x_coastdown` vector. In case Δ`x_coastdown` was [50 30 70], the rider would stop pedaling 50 m before the first stop, 30 m before the second stop, and 70 m before the third stop. For longer coast-downs, it is also possible to set a minimum speed $\dot{x}_{coastdown_{lim}}$, below which the rider will intermittently begin to pedal again, trying to maintain that speed.

The calculation of the braking force is performed through the inversion of Eq. (11), resulting in Eq. (14). The term T_{input} is set to 0 N·m and the other forces are calculated through three blocks equivalent to those reported in Sections (2.3.5–2.3.10-2.3.11).

$$F_{brake} = \frac{T_{input}}{R_c}\cdot\eta_{mec} - F_{clinchers} - F_{slope} - F_{aero_x} - \ddot{x}_{brake_{max}}\cdot k_{inertia} \tag{14}$$

In this model, the braking action is fully dissipative: no energy recovery is accounted for. This simplification of the model tends to return conservative results (i.e., a higher consumption), since it is likely that the velomobile will be equipped with regenerative braking.

2.4. Scenarios: urban vs rural trips

Since no standard cycle has yet been defined for electrically assisted cycles, a set of 1008 scenarios was created in order to obtain a wide range of results encompassing different scenarios inspired by the results of the MoSToVIt survey (Fig. 9).

First, nine main configurations were selected (five for urban trips and four for rural trips). The 9 main itineraries were formed by splitting 2 real trips (one urban and one rural) in various representative segments. Each segment was then assigned different stopping times to simulate various traffic conditions. Then, by varying four parameters (N_{riders}, P_{rider}, α, and Δ`x_coastdown`) the 1008 configurations were formed. Particularly, half of the simulations were run with a single rider ($N_{riders} = 1$), while the other half were set for the tandem configuration ($N_{riders} = 2$). The maximum power input of each rider was set between 50 W and 200 W at intervals of 25 W, to simulate various conditions of low-to-average powering. Higher power output are definitely achievable, but are not so relevant for this study which aims to analyse the behaviour of the velomobile when powered by an average person. Since the slope can affect the performance of the vehicle, the simulations were run with 8 different slope profiles. Only one of these profiles involves a moderate uphill slope (6%), while the others have maximum slopes between -2% and 2%. No simulation was run on moderate downhill since, independently from power input, the velomobile would have reached the speed limit very quickly, shifting the overall average consumption among the simulations towards a very low value, which could have not been

[1] Team Policumbent is a student team of Politecnico di Torino which designs very efficient velomobiles since 2009. Up to this date, the team's fastest bicycles have reached an official speed of 136.4 km/h during the WHPSC competition (at an altitude of about 1400 m, with a slight average downslope of -0.6%), and an unofficial speed of 110 km/h recorded in training on the enclosed track Balocco Proving Ground (at an altitude of 165 m).

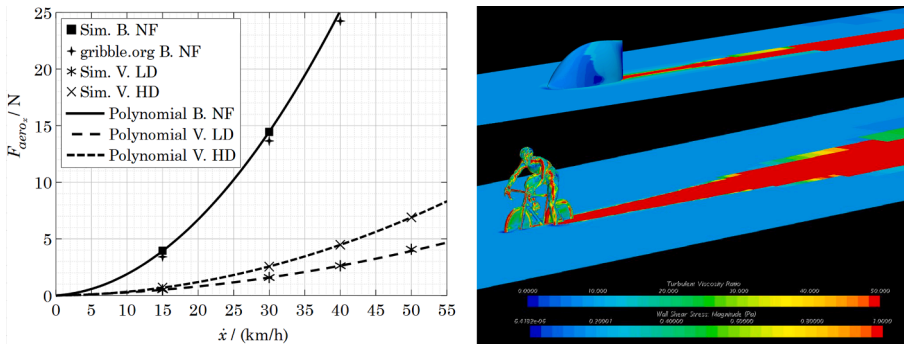

Fig. 8. On the left: curves of aerodynamic resistance for a non-faired bike (B.NF) and for a low and high drag velomobile (V.LD and V.HD respectively). On the right: screenshots from the CFD simulations used to obtain the data points of the aerodynamic resistance at fixed speed.

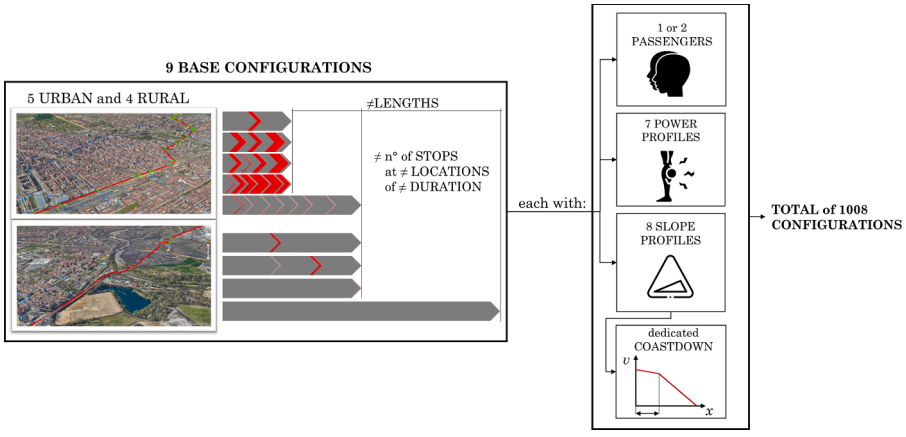

Fig. 9. Procedure to create the itineraries and configurations used for the simulations.

Table 4
Values of the parameters used to set the 1008 simulations.

9 base configurations			
$x_{end\ simulation}$	x_objective	t_still	trip
1000 m	[500] m	[12] s	urban
1000 m	[300 500 800] m	[20 15 30] s	urban
1000 m	[200 350 600 900] m	[12 2 15 30] s	urban
1000 m	[150 400 500 700 850 990] m	[2 15 20 30 30 15] s	urban
2000 m	[200 350 600 900 1100 1300 1600] m	[2 0 0 0 0 0 0] s	urban
2000 m	[800] m	[5] s	rural
2000 m	[800 1500] m	[0 5] s	rural
2000 m	[2000] m	[0] s	rural
4000 m	[] m	[] s	rural

Variable parameters		Constants	
N_{riders}	1, 2	$m_{velomobile}$	45 kg
P_{rider}	50 W, 75 W, 100 W, 125 W, 150 W, 175 W, 200 W	m_{rider}	70 kg
α	constant: − 2%, − 0.5%, 0%, 0.5%, 2%, 6% linear incremental: from 0% to -0.5%, from 0% to 0.5%	P_{motor}	250 W
		$T_{motor_{max}}$	40 N·m
Δx_coastdown	Variable between 0 m and 1000 m, depending on the slope and the trip. See Appendix A for more info	$\ddot{x}_{brake_{max}}$	− 0.5 m/s^2
		$\dot{x}_{coastdown_{lim}}$	12 km/h

considered representative of an average trip.

Table 4 shows a summary of the main configurations and values of the parameters involved in the simulations, while the full results are reported in Appendix A

3. Results and discussion

3.1. Model validation

This section is devoted to the validation of the model presented in Section 2.3. Such validation cannot be performed on the velomobile itself as a physical prototype is not yet available. Nevertheless the authors have used experimental data coming from other kinds of HPVs, i.e. a road bike and a racing handcycle. This validation serves not only to demonstrate the soundness of the model structure but also to show that the model, once fed with experimental data, can effectively become a product-specific digital twin. Such digital twin is especially useful to predict performances and gain insights on the impact of design improvements in racing situations.

The parameters that were changed according to the vehicle simulated are:

- the linear mass of the vehicle m;
- the rotational masses of the wheels I;
- the clincher radius R_c;
- the parameters of the C_d curve;
- the number of teeth of the sprocket's pinions and of the chainring;
- the electric assistance, which was turned off on the road bike and the handcycle.

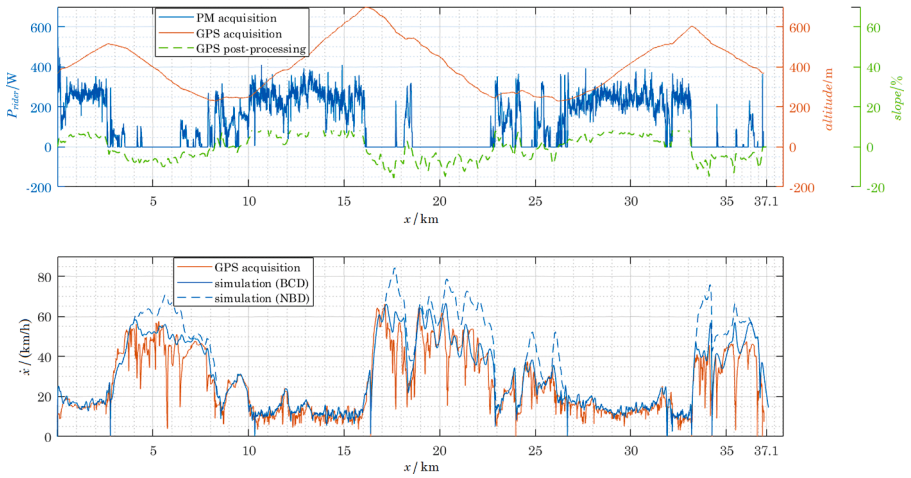

Fig. 10. Model validation - road bike on open road. "BCD": braking correction during descents. "NBD": no braking during descents.

3.1.1. *Road bike - open road test*

The test was conducted on a 37.1 km path which included steep inclines both in ascent and descent. This way, it was possible to simulate the vehicle in various conditions. The power output of the rider was measured with a Favero Assioma Duo (±1% precision, according to the manufacturer [29]). Speed and elevation were detected with a GPS, once per second. The terrain slope was then calculated at 100-m intervals along the entire route, using the GPS data as reference. This last step was critical to minimize the phantom spikes in slope (i.e., non-existing, but detected, especially at low speed). Due to the absence of an apparatus for the measurement of the braking power, first a NBD (No Braking during Descents) simulation was run. Then, assuming reasonable braking powers to avoid fast cornering during the descents, the BCD simulation (Braking Correction during Descents) was run. The maximum speed recorded by the GPS was 66 km, and was reached at the beginning of the 18th km (Fig. 10). A similar situation is repeated at the end of the 19th km. Both events happen at the beginning of a steep downslope, as visible from the green line of the upper graph in Fig. 10. Therefore, excluding the steepest parts of the descents (where the braking power is assumed), all the parameters are known and the speed correlation is good. Along most of the route, only small oscillations are visible. Furthermore, considering the resolution of the GPS on the speed acquisition and the terrain profile uncertainty, such oscillations were to be expected. The model seems to work fine even when the rider applies 400 W of power to the pedals and when there is a sudden increment of 300 W (e.g. at $x = 18\,\text{km}$ and $x = 32\,\text{km}$). These are the orders of magnitude that are expected to be applied to the velomobile during the first part of the acceleration, where the motor could apply up to 250 W of assistance.

3.1.2. *Handcycle - race test*

A second validation was performed with Cerberus, a 3-wheeler arm-powered velomobile designed by team Policumbent of Politecnico di Torino. The data were provided directly by team Policumbent, and concerned an acceleration run of prototype Cerberus on a slight descent. The inputs for the simulation were once again the slope profile and the power input of the rider (this time measured with an SRM PM9 power meter). The instantaneous speed profile of the simulation was then compared with the one recorded onboard of the vehicle. Two different simulations were run, considering a reasonable variability on the drag and rolling resistance coefficients. The experimental data and the results of the simulations are reported in Fig. 11. The correlation is good for most of the race, but there are two discrepancies:

1. There is an undershoot of the speed at the beginning of the simulations. However, this is not a problem and, in fact, tends to produce conservative results.
2. After 70 km/h, the simulations start to diverge from the experimental data, overestimating the speed.

The overall overestimation of the speed can be attributed to three main factors:

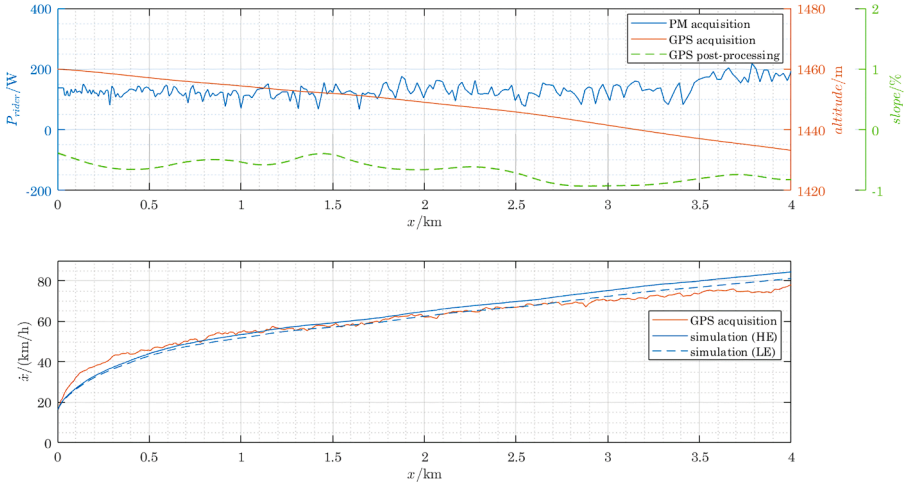

Fig. 11. Model validation - velomobile Cerberus during a speed race. "HE": higher efficiency simulation. "LE": lower efficiency simulation.

1. Actual aerodynamics worse than the simulated one: prototype Cerberus has not been tested in the wind tunnel yet. Previous testing of team a team Policumbent's prototype involved a 2-wheeler. Since Cerberus is a 3-wheeler, it is possible that the actual transition from laminar to turbulent flow starts to occur earlier than expected at high speed.
2. Actual C_{rr} higher than the one used in the simulations: the data used for the C_{rr} curves referred to data recorded on the test bench, whose drum is made of MDF, conversely to the road's asphalt. Furthermore, the asphalt of the road used for the race was reported to be in pretty bad conditions, with holes and even debris on the road [30]. Therefore, the actual C_{rr}, which can have a 15% variability depending on the texture of the asphalt [31], is unknown.
3. There are other dissipative forces that were not accounted for in the model: at higher speed, team Policumbent has reported prototype Cerberus to be quite noisy. This implies that there are vibrational phenomena that have to be reduced in order to minimize the dissipations. For this reason, the overall efficiency of the vehicle may be variable with speed.

However, when compared with the actual speed, the simulated speed remains for most of the run in the range of ±5% error, up to 80 km/h. Since the velomobile that the authors are designing is not expected to go faster, the model seems to be quite adequate for the scope of this paper. Furthermore, in the low-speed range, the model seems to overestimate the dissipations, returning conservative results and setting an upper bound for the expected consumption of the velomobile.

3.2. Expected speed, GHG emissions and energy consumption of the velomobile

As stated in Section 1, the virtual prototype of the velomobile serves a dual purpose:

- Assess the GHG emissions related to the velomobile.
- Verify key design requirements, such as the required speed.

To provide reliable results, the virtual prototype should be tested using boundary conditions representative of the real working conditions. This representativeness is ensured through the methodology presented in Section 2.4. The full results for the 1008 simulations can be found in Appendix A while Table 5 shows a summary of the main results. The GHG emissions of the electric motor where calculated considering the emission factor of 0.3089 g/Wh reported by ISPRA for the Italian electric energy mix [32]. The right part of the table shows the maximum GHG production that can be attributed to the metabolism of the rider, for a vegetarian and an omnivorous diet. The emission factors (1.4 g/kcal and 5.1 g/kcal) were extracted from a literature review on the sustainability of global diets [33]. Particularly, Table 5 shows both the total emissions and its two addenda: one part derives from the increased metabolism due to the physical activity (PA), while one part is related to the basal metabolic rate (BMR). Therefore, the total human emissions should not be blindly compared with well-to-wheel and tank-to-wheel emissions usually reported for the majority of vehicles. A comprehensive comparison of the emissions of this velomobile and other 10 modes of transportation is reported in a companion article of this paper [3]. It is worth to note that all these values are normalised per passenger on board, and per km travelled (p·km, short for passenger·km) in order to be rigorously compared.

Finally, the table also reports the average values for:

- the maximum speed reached during each simulation, and
- the average speed at the end of each simulation

On average, the maximum speed $\dot{x}_{\max}$ for urban trips stands above 30 km/h, and even exceeds 40 km/h for rural trips with flat ground and slight slopes. For urban trips, the average speed is comparable to that of a normal bicycle, since stops and traffic lights do not allow to exploit the superior cruising speed of the velomobile. However, for rural trips, $\dot{x}_{avg}$ generally gets over 30 km/h for average commuters able to generate 100 W continuously (Table 6). With the same power output, on a regular bicycle, a 70 kg commuter using a 12 kg bike would clock a maximum speed of 23–25 km/h [16,17], and the average speed would likely be no more than 20 km/h. On the same bicycle, fitter commuters could reach 30–33 km/h with a power P_{rider} of 200 W. On the velomobile, however, $\dot{x}_{\max}$ would on average go up to 48 km/h, while the average speed for the trip $\dot{x}_{avg}$ would still be notably over 30 km/h for rural trips (Table 7).

These data suggest that the design constraints for the cruising speed on flat ground can be considered satisfied (see Table 2). Moreover, despite its greater mass, thanks to the acceleration provided by the electric motor, the velomobile also results no slower than an average bicycle for urban trips. Being more than 1400 mm tall, the vehicle is also quite visible. It is accessible by two people, who can simultaneously power the transmission in a tandem configuration.

4. Conclusions

This study addresses the development and validation of a virtual prototype capable of quantifying kinematic physical quantities, electric consumption, and GHG emissions during the use phase of Human-Powered Vehicles (HPVs). The validation process, conducted with two different setups, demonstrates a strong correlation between the model's results and experimental data, affirming the reliability and versatility of the proposed model. The validated virtual prototype has been used for two purposes:

- To support the design and development of HPVs, particularly focusing on the velomobile. Additionally, the integration of Model-Based Systems Engineering (MBSE) principles throughout this study underscores the importance of structured methodologies in guiding the design process and ensuring alignment with customer needs.

Table 5
Average values across all the simulations.

Type of trips	Slope subscenario	$\dot{x}_{avg}$ km/h	$\dot{x}_{\max}$ km/h	$e_{e-motor}$ Wh/(p·km)	$GHG_{e-motor}$ g/(p·km)	$GHG_{human,\,TOT}$ g/(p·km)		$GHG_{human,\,PA}$ g/(p·km)		$GHG_{human,\,BMR}$ g/(p·km)	
						veg.	omn.	veg.	omn.	veg.	omn.
Urban	flat only	16.90	32.20	2.25	0.70	31.18	113.60	17.88	65.15	13.30	48.45
	all but 6%	16.86	32.73	2.57	0.80	31.10	113.29	17.72	64.55	13.38	48.75
	all slopes	16.03	30.30	3.83	1.18	35.12	127.95	20.78	75.70	14.34	52.25
Rural	flat only	16.63	30.79	2.37	0.73	29.34	106.87	15.89	57.87	13.45	49.00
	all but 6%	16.60	31.60	2.75	0.85	29.18	106.32	15.65	57.00	13.54	49.32
	all slopes	15.73	29.18	4.09	1.26	33.07	120.47	18.51	67.44	14.56	53.04
Combined	flat only	17.87	36.93	1.70	0.53	37.36	136.08	24.66	89.82	12.70	46.26
	all but 6%	17.75	36.40	1.83	0.56	37.42	136.32	24.61	89.67	12.81	46.65
	all slopes	17.03	33.92	2.77	0.85	41.96	152.85	28.52	103.89	13.44	48.95

Table 6
Results for generic commuters. Average values for simulations run with a power output of $P_{rider} = 100$ W, accounting for both single riders and tandem configurations.

Type of trips	Slope subscenario	$\dot{x}_{avg}$ km/h	$\dot{x}_{max}$ km/h	$e_{e-motor}$ Wh/(p·km)	$GHG_{e-motor}$ g/(p·km)	$GHG_{human,\ TOT}$ g/(p·km)		$GHG_{human,\ PA}$ g/(p·km)		$GHG_{human,\ BMR}$ g/(p·km)	
						veg.	omn.	veg.	omn.	veg.	omn.
Urban	flat only	16.63	30.79	2.37	0.73	29.34	106.87	15.89	57.87	13.45	49.00
	all but 6%	16.60	31.60	2.75	0.85	29.18	106.32	15.65	57.00	13.54	49.32
	all slopes	15.73	29.18	4.09	1.26	33.07	120.47	18.51	67.44	14.56	53.04
Rural	flat only	31.30	38.90	0.46	0.14	20.57	74.92	13.64	49.70	6.92	25.21
	all but 6%	31.96	40.98	1.04	0.32	20.52	74.74	13.48	49.10	7.04	25.64
	all slopes	29.45	37.39	2.58	0.80	24.93	90.83	16.62	60.55	8.31	30.28
Combined	flat only	23.15	34.40	1.52	0.47	25.44	92.67	14.89	54.24	10.55	38.43
	all but 6%	23.42	35.77	1.99	0.62	25.33	92.28	14.68	53.49	10.65	38.79
	all slopes	21.83	32.83	3.42	1.06	29.45	107.30	17.67	64.37	11.78	42.92

Table 7
Results for reasonably fit commuters. Average values for simulations run with a power output of $P_{rider} = 200$ W, accounting for both single riders and tandem configurations.

Type of trips	Slope subscenario	$\dot{x}_{avg}$ km/h	$\dot{x}_{max}$ km/h	$e_{e-motor}$ Wh/(p·km)	$GHG_{e-motor}$ g/(p·km)	$GHG_{h_{TOT}}$ g/(p·km)		$GHG_{h_{PA}}$ g/(p·km)		$GHG_{h_{BMR}}$ g/(p·km)	
						veg.	omn.	veg.	omn.	veg.	omn.
Urban	flat only	17.87	36.93	1.70	0.53	37.36	136.08	24.66	89.82	12.70	46.26
	all but 6%	17.75	36.40	1.83	0.56	37.42	136.32	24.61	89.67	12.81	46.65
	all slopes	17.03	33.92	2.77	0.85	41.96	152.85	28.52	103.89	13.44	48.95
Rural	flat only	38.39	51.68	0.32	0.10	26.37	96.07	20.67	75.28	5.71	20.79
	all but 6%	37.39	49.77	0.50	0.15	26.53	96.66	20.49	74.66	6.04	22.00
	all slopes	34.70	45.62	1.56	0.48	31.94	116.37	25.02	91.14	6.92	25.22
Combined	flat only	26.99	43.48	1.09	0.34	32.47	118.30	22.88	83.36	9.59	34.94
	all but 6%	26.48	42.34	1.24	0.38	32.58	118.69	22.78	83.00	9.80	35.69
	all slopes	24.88	39.12	2.23	0.69	37.51	136.63	26.96	98.23	10.54	38.41

- To quantify the expected emissions associated with velomobile usage, laying the groundwork for a Comparative Life Cycle Assessment presented in a companion paper.

By leveraging the information derived from these simulations, designers can make informed decisions to optimize performance and environmental impact, thereby advancing the adoption of HPVs as a sustainable mode of transportation.

Furthermore, this study highlights and addresses the current gap in standardizing the certification process for the battery range of electrically assisted HPVs. Specifically, the proposed model could be used to simulate the behavior of HPVs in various scenarios, possibly aiding in the identification of a cycle (or cycles) representative of realistic working conditions to be used as a standard. Such cycle(s) may be used not only to assess battery range, offering a valuable tool for users to compare and evaluate velomobile performance, but also to quantify the associated Global Warming Potential (GWP).

In summary, the comprehensive approach taken in this study, from model development to validation and application, positions the proposed virtual prototype as a valuable asset for future battery range/GWP certification processes and design endeavors in the realm of HPVs, contributing to the promotion of environmentally friendly transportation solutions.

CRediT authorship contribution statement

Alessandro Di Gesù: Writing – original draft, Software, Investigation, Data curation, Conceptualization. **Chiara Gastaldi:** Writing – review & editing, Writing – original draft, Validation, Supervision, Project administration, Investigation, Funding acquisition, Data curation, Conceptualization. **Cristiana Delprete:** Writing – review & editing, Supervision, Methodology.

Declaration of competing interest

The authors declare that they have no known competing financial interests or personal relationships that could have appeared to influence the work reported in this article.

Data availability

Data will be made available on request.

Acknowledgments

This study was carried out within the MICS (Made in Italy – Circular and Sustainable) Extended Partnership and received funding from the European Union Next-GenerationEU (PIANO NAZIONALE DI RIPRESA E RESILIENZA (PNRR) – MISSIONE 4 COMPONENTE 2, INVESTIMENTO 1.3 – D.D. 1551.11-10-2022, PE00000004). This manuscript reflects only the authors' views and opinions, neither the European Union nor the European Commission can be considered responsible for them.

Appendix A. Full configurations and simulation results

Refer to file `Appendix-FullConfigurations_and_SimulationResults.ods`

Supplementary material

Supplementary material associated with this article can be found, in the online version, at 10.1016/j.treng.2024.100278

References

[1] T. Wilhelm, V. Dorsch, F. Gauterin, Survey-based accident analysis for human-powered three-wheeled vehicles 10(1) (2021). doi:10.4271/09-10-01-0001.
[2] Accessed 08 August 2023 at 22:03 (CET), https://velomobiel.nl/orderboek/.

[3] A. Di Gesù, C. Gastaldi, C. Delprete, Human-Powered Vehicles as a way to abate Transport-related Greenhouse Gas Emissions: Part 1 - Assessing Modal Shift Impact through Comparative Life Cycle, Assessment - an Italian Case Study (2024).
[4] Eurostat, Urban-rural Europe - introduction, Accessed 07 August 2023 at 11:45 (CET), https://ec.europa.eu/eurostat/statistics-explained/index.php?title=Urban-rural_Europe_-_introduction.
[5] E.W. Faria, D.L. Parker, I.E. Faria, The science of cycling: factors affecting performance - Part 2 35(4) (2005) 313–337. doi:10.2165/00007256-200535040-00003.
[6] D. Meyer, G. Kloss, V. Senner, What is slowing me down? Estimation of rolling resistances during cycling 147 (2016) 526–531. doi:10.1016/j.proeng.2016.06.232.
[7] T.N. Crouch, D. Burton, Z.A. LaBry, K.B. Blair, Riding against the wind: a review of competition cycling aerodynamics 20 (2) (2017) 81–110, https://doi.org/10.1007/s12283-017-0234-1.
[8] D.J. Wagg, K. Worden, R.J. Barthorpe, P. Gardner, Digital twins: state-of-the-art and future directions for modeling and simulation in engineering dynamics applications 6(3) (2020). doi:10.1115/1.4046739.
[9] O. San, S. Pawar, A. Rasheed, Decentralized digital twins of complex dynamical systems 13(1) (2023). doi:10.1038/s41598-023-47078-9.
[10] L. Hadjidemetriou, N. Stylianidis, D. Englezos, P. Papadopoulos, D. Eliades, S. Timotheou, M.M. Polycarpou, C. Panayiotou, A digital twin architecture for real-time and offline high granularity analysis in smart buildings 98(2023) 104795. doi:10.1016/j.scs.2023.104795.
[11] J. Lee, J. Ni, D. Djurdjanovic, H. Qiu, H. Liao, Intelligent prognostics tools and e-maintenance 57(6) (2006) 476–489. doi:10.1016/j.compind.2006.02.014.
[12] A. Cerrone, J. Hochhalter, G. Heber, A. Ingraffea, On the effects of modeling as-manufactured geometry: toward digital twin 2014 (2014) 1–10. doi:10.1155/2014/439278.
[13] B.R. Seshadri, T. Krishnamurthy, Structural health management of damaged aircraft structures using digital twin concept. 25th AIAA/AHS Adaptive Structures Conference, American Institute of Aeronautics and Astronautics, 2017, https://doi.org/10.2514/6.2017-1675.
[14] E. Brusa, A. Calá, D. Ferretto, Systems Engineering and Its Application to Industrial Product Development, Springer International Publishing, 2018, https://doi.org/10.1007/978-3-319-71837-8.
[15] G.K. Walden, Systems engineering handbook of INCOSE, 2015.
[16] B. Szyk, Å. Zaborowska, Cycling wattage calculator, Accessed 05 August 2023 at 17:03 (CET), https://www.omnicalculator.com/sports/cycling-wattage.
[17] S. Gribble, Cycling power and speed, Accessed 05 August 2023 at 17:13 (CET), https://www.gribble.org/cycling/power_v_speed.html.
[18] D. Badau, G. Prebeg, D. Mitić, A. Badau, Fitness index and vo2max of physical education students 15 (2015) 246–251.
[19] M.A. Van Baak, R.A. Binkhorst, Oxygen consumption during outdoor recreational cycling 24(9) (1981) 725–733. doi:10.1080/00140138108924894.
[20] P. Baldissera, C. Delprete, Rolling resistance, vertical load and optimal number of wheels in human-powered vehicle design 231(1) (2016) 33–42. doi:10.1177/1754337115625002.
[21] C.R. Kyle, F. Berto, The mechanical efficiency of bicycle derailleur and hub-gear transmissions (52) (2001) 3–11. https://forum.bhpc.org.uk/uploads/1178/hp52-2001.pdf.
[22] B. Rohloff, P. Greb, C. Kyle, Efficiency Measurements of Bicycle Transmissions - a neverending Story? (55) (2004) 11–15. http://www.whpva.org/HParchive/hp55p11-15.pdf.
[23] P. Baldissera, C. Delprete, From pbl to innovation: a decennial case-study from an hpv student team 18(4) (2020) 773–786. doi:10.1108/jedt-01-2019-0005.
[24] outrider usa, https://outriderusa.com/pages/electric-bike-efficiency.
[25] Science2Sport, Performing and analysing torque intervals, 2018. https://bikehub.co.za/news/performing-and-analysing-torque-intervals-r7368/.
[26] P. Baldissera, C. Delprete, M. Rossi, A. Zahar, Experimental comparison of speed-dependent rolling coefficients in small cycling tires 49(3) (2020) 224–241. doi:10.2346/tire.20.190207.
[27] T. Policumbent, A blast of wind for Taurus, 2018. https://www.policumbent.it/en/blog/a-blast-of-wind-for-taurus/.
[28] T. Policumbent, Estimating the drag coefficient from experimental data, 2018. https://www.policumbent.it/en/blog/estimating-the-drag-coefficient-basing-on-experimental-data/.
[29] F. Electronics, 0259-0902A Assioma user manual_Rev19 - EN-IT-DE, https://cache.tradeinn.com/images/pdf/manuales/eng_favero_manu_assioma.pdf.
[30] Whpsc 2023: Tuesday pm results, 2023. https://jnyyz.wordpress.com/2023/09/13/whpsc-2023-tuesday-p-results/.
[31] J.A. Ejsmont, G. Ronowski, B. Świeczko-Żurek, S. Sommer, Road texture influence on tyre rolling resistance 18(1) (2016) 181–198. doi:10.1080/14680629.2016.1160835.
[32] A. Caputo, Efficiency and decarbonization indicators in Italy and in the biggest European Countries. Edition 2023, Istituto Superiore per la Protezione e la Ricerca Ambientale (ISPRA), 2023.https://www.isprambiente.gov.it/files2023/pubblicazioni/rapporti/r386-2023.pdf
[33] D. Tilman, M. Clark, Global diets link environmental sustainability and human health 515(7528) (2014) 518–522. doi:10.1038/nature13959.